

Smith-Purcell radiation from time grating

Juan-Feng Zhu,¹ Ayan Nussupbekov,² Wenjie Zhou,^{1,3} Zicheng Song,⁴ Xuchen Wang,⁵ Zi-Wen Zhang,⁶ Chao-Hai Du,⁶ Ping Bai,² Ching Eng Png,² Cheng-Wei Qiu,^{3,*} and Lin Wu^{1,2,†}

¹*Science, Mathematics, and Technology (SMT), Singapore University of Technology and Design (SUTD), 8 Somapah Road, Singapore 487372.*

²*Institute of High Performance Computing, A*STAR (Agency for Science, Technology, and Research), 1 Fusionopolis Way, No. 16-16 Connexis, Singapore 138632.*

³*Department of Electrical and Computer Engineering, National University of Singapore, 4 Engineering Drive 3, Singapore 117583.*

⁴*Center for Composite Materials and Structures, School of Astronautics, Harbin Institute of Technology, Harbin 150080, China.*

⁵*Institute of Nanotechnology, Karlsruhe Institute of Technology, Karlsruhe, Germany*

⁶*Optical Communication Systems and Networks, School of Electronics, Peking University, Beijing, 100871, P. R. China*

Smith-Purcell radiation (SPR) occurs when an electron skims above a spatial grating, but the fixed momentum compensation from the static grating imposes limitations on the emission wavelength. It has been discovered that a temporally periodic system can provide energy compensation to generate light emissions in free space. Here, we introduce temporal SPR (t -SPR) emerging from a time grating and propose a generalized t -SPR dispersion equation to predict the relationship between radiation frequency, direction, electron velocity, modulation period, and harmonic orders. Compared to conventional SPR, t -SPR can: 1) Provide a versatile platform for manipulating SPR emission through temporal modulation (*e.g.*, period, amplitude, wave shape). 2) Exhibit strong robustness to the electron-grating separation, alleviating the constraints associated with extreme electron near-field excitation. 3) Introduce additional energy channels through temporal modulation, enhancing and amplifying emission.

Smith-Purcell radiation (SPR) arises when fast-moving charged particles travel above a spatially periodic grating. This phenomenon was initially elucidated by D. H. Smith and E. M. Purcell during the 1950s [1] and has since discovered a plethora of applications spanning diverse fields, including vacuum electronic devices [2], particle accelerators [3], and free-electron lasers [4]. In recent years, SPR has achieved remarkable advancements by replacing conventional gratings with metamaterials [5, 6], enabling comprehensive control over its coherence, polarization, and radiation direction [7–13]. In particular, novel and captivating optical phenomena such as bound states in the continuum [14] and flat-band resonances [15] have been harnessed to significantly enhance the intensity of SPR. Nevertheless, till today, all development still relies on “momentum compensation” facilitated by spatial modulations and energy of free electron.

A special type of metamaterial, time-varying metamaterial, whose physical properties change over time, provides additional degrees of freedom in the time domain for manipulating interactions with light waves, beyond the conventional three-dimensional space [16, 17]. In contrast to spatial interfaces, momentum is conserved at temporal boundaries [18] instead of energy, because external energy is required to modulate the material properties, leading to changes in the electromagnetic energy within the system. Time-varying metamaterials have already demonstrated exciting applications, including time reversal [19], nonreciprocity [20, 21], temporal aiming [22], and even more fascinating possibilities on the hori-

zon [23–27]. In particular, photonic time crystal (PTC) can be created by implementing temporal periodic modulation in uniform materials [28]. Analogous to photonic crystals, the temporal periodic modulation leads to interference in time reflections and refractions, giving rise to the creation of bands and bandgaps in momentum. What’s particularly exciting is the revelation of the exponential energy growth within the PTC momentum gap, providing opportunities for achieving light amplification [29, 30]. It’s worth noting that the periodic temporal modulation induces frequency harmonic waves rather than momentum harmonic waves, thus offering a versatile platform for light manipulation. For instance, the propagating wave can be coupled to near-field surface waves along the time-grating surface through frequency down-conversion [31]. The temporal modulation provides additional energy to allow free electrons to induce the Cherenkov radiation (CR) within the PTC, even with mismatched energy threshold [32].

Inspired by the work of CR in PTC [32], we propose the concept of temporal SPR (t -SPR) from a time grating (TG) as illustrated in Fig. 1, an analogy to the conventional spatial SPR (s -SPR) from a spatial grating. When the free electron flies above the TG, owing to the frequency harmonic wave, the t -SPR can be stimulated over a broad frequency range. In this Letter, we aim to extend physics concepts of conventional s -SPR to t -SPR. We first derive the dispersion equation for t -SPR to reveal the relationship between the radiation frequency f , radiation direction θ , the normalized electron veloc-

ity β , and harmonic order m . We then employ full-wave electromagnetic simulations to verify our derived dispersion equation. To engineer the characteristics of t -SPR (benchmark to s -SPR), we study the conditions for maximizing its radiation intensity, in terms of internal factor (*e.g.*, electron-grating separation d , normalized electron velocity β) and external factor (*e.g.*, time modulation function, period, amplitude). We hope to open a new research pursuit toward “active” free-electron light sources enabled by material temporal modulation, beyond the state-of-the-art spatial methods.

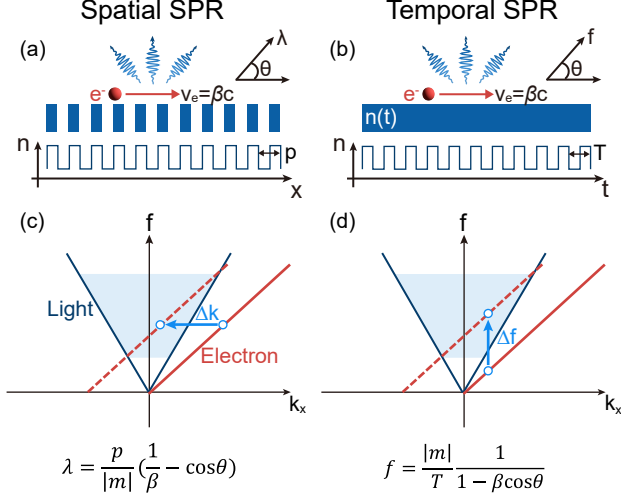


FIG. 1. Spatial SPR (s -SPR) vs. temporal SPR (t -SPR). Schematics of (a) s -SPR or (b) t -SPR, induced when a swift free electron flies (with a speed of v_e) above (a) a grating with refractive index n changing along the x -space with a period of p , or (b) a time grating with n changing with time t at a period of T . Dispersion diagrams for (c) s -SPR and (d) t -SPR where blue lines indicate light cone. Diffracted by (c) the momentum harmonic wave from the space grating, or (d) the frequency harmonic wave from the TG, the electron dispersion curve (red solid line) shifts (c) left/right along the k_x -axis as energy is conserved, or (d) upward/downward along the f -axis as momentum is conserved. The s -SPR and t -SPR are characterized by emission wavelength (λ) or frequency (f) and emission angle (θ), which are determined by the normalized electron velocity ($\beta = v_e/c$) and modulation period (p or T) following the shown generalized dispersion equations.

Without losing generality, s -SPR is introduced first. As depicted in Fig. 1(a), s -SPR is induced when a free electron skims over a spatial grating (refractive index n is modulated periodically as a function of x) with a velocity $v_e = \beta c$ along the x direction. To illustrate the mechanism, the momentum-frequency dispersion diagram is analyzed in Fig. 1(c), where blue line indicates the light cone. The dispersion relation of the free electron can be expressed as $\omega = v_e k_{xe}$ (red solid line), where k_{xe} is the propagation wavenumber along the x -axis. Since $v_e < c$, we have $k_{xe} > k_0$ with k_0 the free space wavenumber, im-

plying that the electromagnetic wave carried by the free electron is evanescent. Spatial grating provides the free electron with momentum compensation: $\Delta k_x = 2\pi m/p$, where m denotes the diffraction order, and p is the period of grating. Consequently, the dispersion curve for the free electron can be shifted left ($m < 0$) or right ($m > 0$) along the k_x -axis, as exemplified by the blue arrow in Fig. 1(c). When the electron dispersion curve shifts above the light cone (red dashed line), the evanescent wave can diffract into a propagating wave in free space. The corresponding radiation frequency range can be determined by the intersection points between the dispersion curve of the electron and the light cone (blue region). The classic dispersion relation between radiation frequency (or wavelength $\lambda = c/f$) and angle (θ) can be obtained via the momentum-matching conditions:

$$\lambda = \frac{p}{|m|} \left(\frac{1}{\beta} - \cos \theta \right). \quad (1)$$

On the other hand, when the materials properties, *e.g.*, refractive index n of a uniform dielectric slab, vary periodically with respect to time instead of space, a TG is created in Fig. 1(b). According to Bloch-Floquet theorem, the electric profiles of TG can be expanded by Fourier series: $E(t) = \sum_m e_m e^{j(\omega - m\Omega)t}$, where $\Omega = 2\pi f_m$ with $f_m = 1/T$ the modulation frequency and T the modulation period, and $m = 0, \pm 1, \pm 2, \dots$ is the harmonic order, immediately suggesting that the temporal harmonic modulation will alter the operation frequency [33].

When a free electron hovers above TG (grating/free-space interface at $z = 0$) with a separation distance d , the excitation of the free electron is given by $J(x, z, t) = \hat{x} q v_e \delta(z-d) \delta(x - v_e t)$, and the frequency domain expression is obtained through Fourier transform $J(x, z, \omega) = \hat{x} q \delta(z-d) e^{j\omega t} e^{-jk_{xe}x}$, where $k_{xe} = \omega/v_e$. Hence, the evanescent wave induced by the free electron source can be written as:

$$H_y^i = \hat{y} A_0 e^{j\omega t} e^{-jk_{xe}x - jk_{z0}(z-d)}, \quad (2)$$

$$E_x^i = -\hat{x} A_0 \frac{k_{xe}x}{\omega \varepsilon_0} e^{j\omega t} e^{-jk_{xe}x - jk_{z0}(z-d)}. \quad (3)$$

where A_0 is the electron amplitude. The reflected wave in the free space ($z > 0$) is:

$$H_y^r = \hat{y} \sum_m R_m e^{j\omega t} e^{-jk_{xe}x - jk_{zm}z}, \quad (4)$$

$$E_x^r = \hat{x} \sum_m R_m \frac{k_{xe}}{(\omega - m\Omega)\varepsilon_0} e^{j(\omega - m\Omega)t} e^{-jk_{xe}x - jk_{zm}z}, \quad (5)$$

where $k_{xe}^2 + k_{zm}^2 = k_m^2 = [(\omega - m\Omega)/c]^2$. Eqs. (4)-(5) indicate that the frequency harmonic wave is induced by TG. Thus the electron dispersion line (red solid line)

shifts either upward (for $m < 0$) or downward (for $m > 0$) along the f -axis in Fig. 1(d). Likewise, when the electron dispersion line moves above the light cone (red dashed line), the evanescent wave is converted into the plane wave in the far-field and gives rise to the t -SPR. The corresponding dispersion curve can be expressed as follows (see SI-1 [34] for derivation):

$$f = \frac{|m|}{T} \frac{1}{1 - \beta \cos \theta}. \quad (6)$$

This equation reveals that the frequency of t -SPR can be customized by the modulation period T and spans a frequency band for the m^{th} frequency harmonic wave:

$$\frac{|m|}{1 + \beta T} < f < \frac{|m|}{1 - \beta T}. \quad (7)$$

To verify this dispersion relation, we run two dimensional time-domain numerical simulations and perform Fourier transformation (see SI-2 [34]) to vividly unveil the characteristics of t -SPR in Fig. 2. We set our refractive index modulation function as $n(t) = A \cdot W(t) + n_a$, where A denotes the amplitude, $W(t)$ represent the shape of the modulation function with $f_m = 1/T$ the modulation frequency, and n_a is the central refractive index. We choose the following parameters throughout this study unless otherwise mentioned: $A = 0.2$, $n_a = 1.5$, $f_m = 20$ GHz, W is in a square waveform; normalized electron velocity $\beta = 0.2$, and electron-grating separation $d = 0.5$ mm.

As shown in Fig. 2(a), when the electron flies over the TG, it generates radiations both within free space and within the TG. Upon removing the temporal modulation, both radiations become imperceptible, indicating the crucial role played by temporal modulation. To gain insight into the underlying mechanisms, we plot the dispersion diagram in Fig. 2(b). Here, the dispersion curve of TG (orange line) is derived by matching the temporal boundaries, which exhibits momentum gaps occurring at integer multiple frequencies of $0.5f_m$ (see SI-3 [34]). Within the momentum gap, the wave experiences exponential growth over time due to the extra energy injected into the system through modulation [28, 29, 32]. The asymptotic light line in TG can also be expressed as $\omega = ck_x/n_{\text{eff}}$, with n_{eff} denoting the effective refractive index of TG [35]. Meanwhile, the frequency harmonic dispersion curve of the free electron shifts either upward or downward with distance mf_m along the f -axis. For example, the case of $m = -1$ is considered (red dashed); this -1^{st} harmonic wave transits above the free-space light cone, generating an overlapping area depicted as the blue region. It indicates the conversion of the evanescent wave of the free electron into a propagating wave in the far field, thereby giving rise to t -SPR. Simultaneously, this -1^{st} harmonic wave reaches above TG light cone, leading to an overlapping area depicted as the grey re-

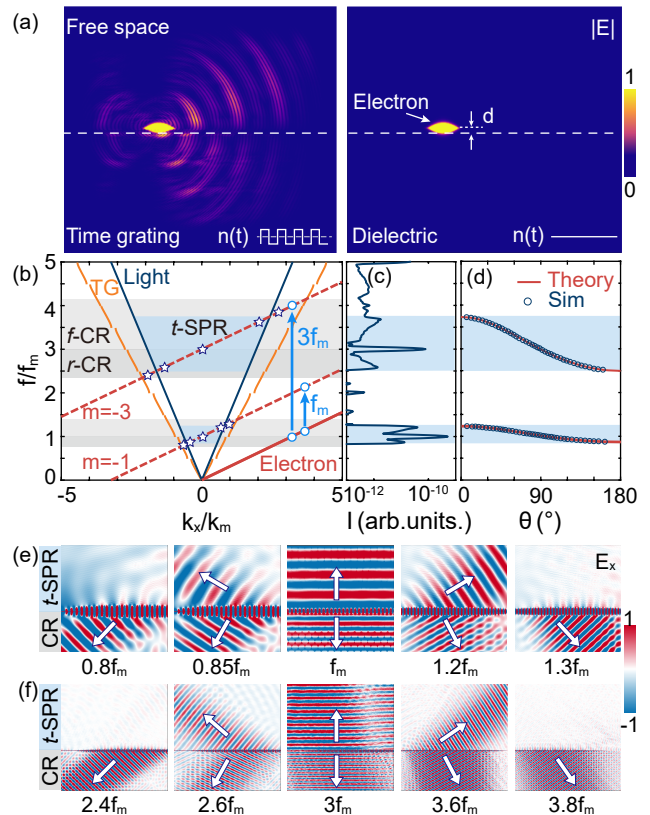


FIG. 2. Mechanism investigations on the simultaneous excitation of t -SPR and CR in an exemplified system with the normalized electron velocity $\beta = 0.2$ and square temporal modulation with $f_m = 20$ GHz. (a) Field intensity profiles in time domain when a free electron flies over a dielectric slab with or without a temporal modulation. Left: t -SPR (and CR) is induced in the free space (and dielectric slab) with the temporal modulation. Right: no radiation is observed upon removal of temporal modulation. (b) The dispersion diagram of the exemplified system: light line (blue), energy band within TG (orange), electron (solid red), and electron harmonic wave (dashed red). The radiation frequency range can be determined by the intersection points between the electron harmonic wave and the light line for t -SPR (blue region); or between the electron harmonic wave and TG line for forward-CR (f -CR) and reverse-CR (r -CR) (grey regions). (c) The t -SPR radiation spectrum probed in the free space. (d) The relation between radiation angle (θ) and frequency for t -SPR: theory (solid line) and simulations (symbols). (e)-(f) Simulated electric-field profiles at selected frequencies marked by stars in (b) for 1^{st} ($m = -1$) and 3^{rd} ($m = -3$) harmonic orders, where the arrows indicate the directions of t -SPR and CR in different scenarios.

gion, indicating the conversion into a propagating wave into TG.

Fig. 2(c) presents the simulated radiation spectrum. As the TG shifts the electron harmonic line upward along the f -axis, the radiation characteristics at frequency f rely on the evanescent wave at the frequency $f - f_m$. Serving as the intrinsic evanescent wave of the free elec-

tron wave, the decay distance increases as the frequency decreases while maintaining a constant velocity according to Bohr cutoff distance, $d_{\text{Bohr}} = \beta / (2\pi f \sqrt{1 - \beta^2})$, the length scale over which the moving electron's evanescent field decays exponentially with transverse distance from its axis of motion [36, 37]. The electric intensity interacting with the TG becomes stronger as the operational frequency approaches zero. Consequently, the radiation spectrum reaches its peak at f_m and subsequently diminishes as f deviates from f_m .

In addition, Eq. (6) predicts a relationship between the radiation angle (θ) and frequency (f), which is shown in Fig. 2(d) (line). As suggested, t -SPR exhibits a beam-scanning characteristic within the operation bandwidth. The radiation direction switches from backward (180° - 90°) to forward (90° - 0°) as f increases and a normal emission is produced at $f = f_m$. This relationship has been validated by our simulations in Fig. 2(d) (symbols) and vividly illustrated by the electric-field profiles at selected f in Fig. 2(e): $0.85f_m$ (backward), f_m (normal), $1.2f_m$ (forward). Moreover, t -SPR ceases to appear outside the predicted t -SPR range ($0.83f_m < f < 1.25f_m$) according to Eq. (7).

Interestingly, along with t -SPR excitation, there exist radiation within TG, which we account for CR due to the phase velocity of -1^{st} harmonic wave exceeding that of light within TG as clearly evidenced in Fig. 2(b). The CR frequency range can be divided into two regions by the line $f = f_m$: reverse-CR (r -CR) and forward-CR (f -CR), which manifest in the left ($k_x < 0$) and right ($k_x > 0$) half-spaces, respectively, signifying the energy flow propagates backwardly or forwardly with respect to the electron motion. As depicted in Fig. 2(e), r -CR is evident at $0.8f_m$ and $0.85f_m$, while f -CR is observed at $1.2f_m$ and $1.3f_m$. In particular, r -CR serves to separate electrons from the wake fields they generate, offering a wide range of applications in the high-energy particle field [38, 39]. Traditionally, r -CR can be produced within double-negative metamaterials [40]; here, the TG introduces a novel approach to its generation. It's important to note that the electron energy in our setup ($\beta = 0.2$) is considerably lower than the minimum CR threshold ($\beta_{\text{CR}} = 1/1.7 \approx 0.59$). Periodic temporal modulation provides the necessary energy boost for electrons to surpass the threshold required to induce CR [32]. It represents an exceptional solution to a long-standing challenge in eliminating the CR threshold besides the hyperbolic metamaterials [41]. When electron energy is sufficiently high and surpasses the minimum energy threshold within TG (e.g., $\beta = 0.6$), CR can be directly induced, both fundamental wave ($m = 0$) and higher-order harmonics ($|m| > 0$) come into play (see SI-4 [34]).

Similar to conventional s -SPR, t -SPR also exhibits characteristics of high-order harmonic radiation. For instance, the 3^{rd} harmonic radiation around $f = 3f_m$ is illustrated in Fig. 2(b). The radiation angle, as observed

by the numerical simulations, closely aligns with theoretical expectations. However, in comparison to the 1^{st} order radiation, the intensity is noticeably diminished due to the declining harmonic intensity with increasing orders [42, 43]. Nevertheless, it provides a potential pathway towards achieving frequency up-conversion and may find applications in the realm of extreme frequency lasing, especially in the ultraviolet range [44]. It's worth noting that the radiation spectrum near $2f_m$ is much weaker in this case, primarily because of the weak 2^{nd} harmonic amplitude [42].

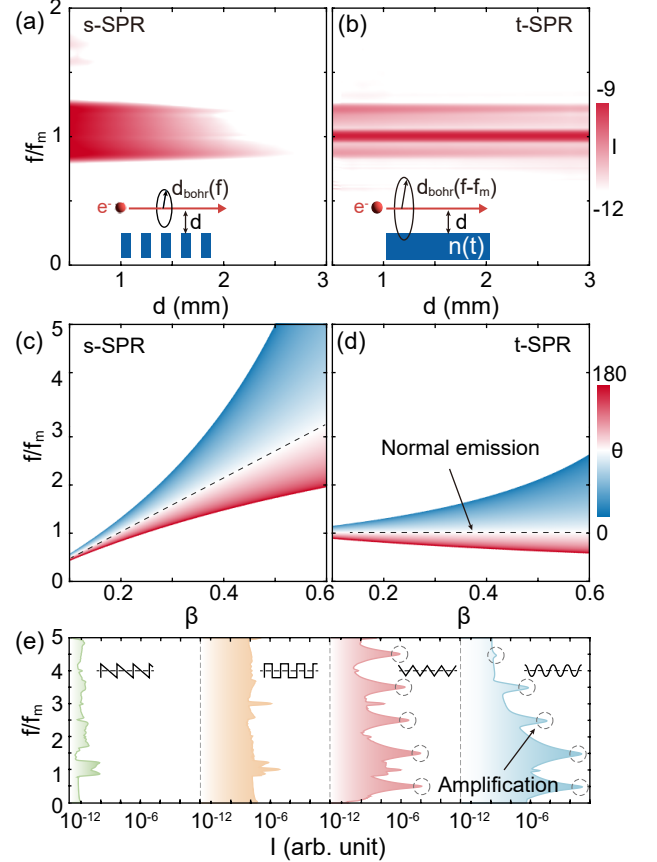


FIG. 3. Quantitative analysis for 1^{st} order s -SPR and t -SPR. The dependence of emission intensity spectra on electron-grating separation d for (a) s -SPR or (b) t -SPR. Tuning radiation direction by varying electron velocity β for (c) s -SPR or (d) t -SPR. (e) Active control on t -SPR by changing the shape of temporal modulation function $W(t)$.

In both s -SPR and t -SPR, the conversion of the electron's evanescent wave into free-space radiation is facilitated through the compensation of momentum or energy from the spatial or time grating, respectively. Their characteristics exhibit several distinctions, and a direct comparison is detailed in Fig. 3. To ensure that s -SPR and t -SPR encompass the same radiation range, it is crucial to maintain a specific relationship between the spatial and temporal periods, denoted as $p = T\beta c$, while consid-

ering the same working harmonic order (see SI-5 [34]). It's worth noting that the evanescent field of a moving electron experiences exponential decay with increasing transverse distance, *i.e.*, d_{Bohr} , and the proximity of the electron trajectory to the grating surface d plays a pivotal role [37]. In general, closer distances result in stronger interactions. However, this distance is constrained by experimental resolution to prevent direct electron impact on the structure for conventional *s*-SPR. In contrast, *t*-SPR demonstrates robustness to electron-grating separation d . With increased d , the intensity of *s*-SPR exponentially decreases (Fig. 3(a)), while that of *t*-SPR remains relatively constant (Fig. 3(b)), which highlights their distinct excitation mechanisms. The intensity at the same radiation frequency f is determined by the amplitude of frequency harmonic wave at $f - f_m$ for *t*-SPR but f for *s*-SPR. Due to the much longer Bohr cutoff distance $d_{\text{Bohr}}(f - f_m)$ compared to $d_{\text{Bohr}}(f) = 0.48$ nm, *t*-SPR becomes relatively insensitive to electron-grating separation in the studied range of 0.5 – 3 nm. This alleviates the constraints of electron operation within the near-field [45]. Additionally, we compare the radiation angle distributions for *s*-SPR and *t*-SPR in Fig. 3(c)-(d) by tuning the normalized electron velocity β and reveal that normal emission ($\theta = 90^\circ$) consistently occurs at f_m with varying β for *t*-SPR. This consistency is attributed to the fact that the radiation frequency f_m remains steadfast along the f -axis, regardless of variations in β , and is accompanied by a corresponding wavenumber of $k_x = 0$. This feature highlights a potential application in frequency-locked light sources [7, 46].

Of particular significance, *t*-SPR offers several noteworthy advantages concerning energy and reconfigurability. **First**, in *s*-SPR, a spatial grating functions as a passive system, adhering to the principles of energy conservation. It converts the evanescent waves carried by electrons into spatially propagating waves, with the total system energy being derived exclusively from the electrons. Conversely, *t*-SPR in TG operates as an active system, departing from strict adherence to energy conservation principles within the system. It has the capacity to introduce external energy through temporal modulation and transfer this energy to the electron-photon interaction, thus sidestepping conventional energy conservation constraints. Consequently, *t*-SPR introduces an additional energy channel with the potential to significantly enhance the radiation intensity. For example, when our external modulations are appropriately configured (the triangular or cosine modulation function as shown in Fig. 3(e)), the amplification effect becomes evident at frequency $(2N + 1)f_m/2$ where N is an integer, consistent with findings from recent CR in PTC literature [32]. The leaking amplified wave contributes to the enhancement of *t*-SPR intensity. Functioning as an active amplification mechanism, *t*-SPR shows potential as a platform for on-chip electron accelerators with the precise

matching of the phase conditions between the electron and the *t*-SPR wave [47–49]. **Second**, *t*-SPR provides a reconfigurable platform. In *s*-SPR, the emission characteristics are contingent upon the electron energy with the fabricated grating. In contrast, the TG allows for adaptability through the adjustment of the modulation period T , amplitude A (see SI-6 [34]), and modulation functions $W(t)$ [50]. This attribute holds significant promises for the development of advanced active free-electron light sources and versatile system configurations.

In conclusion, we present a theoretical prediction of *t*-SPR from free electron traveling atop a simple TG. Looking forward, we aim to stimulate experimental verification with the key task of achieving high-speed modulation for the TG. Potential platforms for experimentation include graphene and epsilon-near-zero films, such as indium tin oxide [20, 51]. The consideration of TG with finite thickness is also paramount, and comprehensive information regarding this aspect can be found in SI-7 [34]. Analogous to *s*-SPR originating from a transmission grating, *t*-SPR can be detected in both the top and bottom half-spaces, following our derived radiation directions based on Eq. (6).

This work was supported by the Singapore University of Technology and Design for the Start-Up Research Grant SRG SMT 2021 169 and Kickstarter Initiative (SKI) SKI 2021-02-14, and National Research Foundation Singapore via Grant No. NRF2021-QEP2-02-P03, NRF2021-QEP2-03-P09, and NRF-CRP26-2021-0004.

* chengwei.qiu@nus.edu.sg

† lin.wu@sutd.edu.sg

- [1] S. J. Smith and E. Purcell, *Physical Review* **92**, 1069 (1953).
- [2] R. P. Leavitt, D. E. Wortman, and C. A. Morrison, *Applied Physics Letters* **35**, 363 (1979).
- [3] E. A. Nanni, W. R. Huang, K.-H. Hong, K. Ravi, A. Fallahi, G. Moriena, R. Dwayne Miller, and F. X. Kärtner, *Nature Communications* **6**, 8486 (2015).
- [4] J. Urata, M. Goldstein, M. Kimmitt, A. Naumov, C. Platt, and J. Walsh, *Physical Review Letters* **80**, 516 (1998).
- [5] Z. Su, B. Xiong, Y. Xu, Z. Cai, J. Yin, R. Peng, and Y. Liu, *Advanced Optical Materials* **7**, 1801666 (2019).
- [6] C. Roques-Carmes, S. E. Kooi, Y. Yang, N. Rivera, P. D. Keathley, J. D. Joannopoulos, S. G. Johnson, I. Kaminer, K. K. Berggren, and M. Soljačić, *Applied Physics Reviews* **10** (2023).
- [7] S. Korbly, A. Kesar, J. Sirigiri, and R. Temkin, *Physical Review Letters* **94**, 054803 (2005).
- [8] Z. Wang, K. Yao, M. Chen, H. Chen, and Y. Liu, *Physical Review Letters* **117**, 157401 (2016).
- [9] Z. Su, F. Cheng, L. Li, and Y. Liu, *ACS Photonics* **6**, 1947 (2019).
- [10] I. Kaminer, S. Kooi, R. Shiloh, B. Zhen, Y. Shen, J. López, R. Remez, S. Skirlo, Y. Yang, J. Joannopoulos,

- et al.*, *Physical Review X* **7**, 011003 (2017).
- [11] L. Jing, X. Lin, Z. Wang, I. Kaminer, H. Hu, E. Li, Y. Liu, M. Chen, B. Zhang, and H. Chen, *Laser & Photonics Reviews* **15**, 2000426 (2021).
- [12] L. Jing, Z. Wang, X. Lin, B. Zheng, S. Xu, L. Shen, Y. Yang, F. Gao, M. Chen, and H. Chen, *Research* (2019).
- [13] Z.-W. Zhang, J.-F. Zhu, C.-H. Du, F. Gao, F.-Y. Han, and P.-K. Liu, *Laser & Photonics Reviews* **17**, 2200420 (2023).
- [14] Y. Yang, A. Massuda, C. Roques-Carmes, S. E. Kooi, T. Christensen, S. G. Johnson, J. D. Joannopoulos, O. D. Miller, I. Kaminer, and M. Soljačić, *Nature Physics* **14**, 894 (2018).
- [15] Y. Yang, C. Roques-Carmes, S. E. Kooi, H. Tang, J. Beroz, E. Mazur, I. Kaminer, J. D. Joannopoulos, and M. Soljačić, *Nature* **613**, 42 (2023).
- [16] N. Engheta, *Science* **379**, 1190 (2023).
- [17] R. Fante, *IEEE Transactions on Antennas and Propagation* **19**, 417 (1971).
- [18] H. Moussa, G. Xu, S. Yin, E. Galiffi, Y. Ra'di, and A. Alù, *Nature Physics* **19**, 863 (2023).
- [19] V. Bacot, M. Labousse, A. Eddi, M. Fink, and E. Fort, *Nature Physics* **12**, 972 (2016).
- [20] D. L. Sounas and A. Alù, *Nature Photonics* **11**, 774 (2017).
- [21] X. Guo, Y. Ding, Y. Duan, and X. Ni, *Light: Science & Applications* **8**, 123 (2019).
- [22] V. Pacheco-Peña and N. Engheta, *Light: Science & Applications* **9**, 129 (2020).
- [23] V. Pacheco-Peña and N. Engheta, *Optica* **7**, 323 (2020).
- [24] R. Tirole, S. Vezzoli, E. Galiffi, I. Robertson, D. Maurice, B. Tilmann, S. A. Maier, J. B. Pendry, and R. Sapienza, *Nature Physics* **19**, 999–1002 (2023).
- [25] E. Galiffi, G. Xu, S. Yin, H. Moussa, Y. Ra'di, and A. Alù, *Nature Physics* **19**, 1703–1708 (2023).
- [26] K. Lee, J. Son, J. Park, B. Kang, W. Jeon, F. Rotermund, and B. Min, *Nature Photonics* **12**, 765 (2018).
- [27] D. Oue, K. Ding, and J. Pendry, *Physical Review Research* **4**, 013064 (2022).
- [28] E. Lustig, Y. Sharabi, and M. Segev, *Optica* **5**, 1390 (2018).
- [29] M. Lyubarov, Y. Lumer, A. Dikopoltsev, E. Lustig, Y. Sharabi, and M. Segev, *Science* **377**, 425 (2022).
- [30] X. Wang, M. S. Mirmoosa, V. S. Asadchy, C. Rockstuhl, S. Fan, and S. A. Tretyakov, *Science Advances* **9**, eadg7541 (2023).
- [31] E. Galiffi, Y.-T. Wang, Z. Lim, J. B. Pendry, A. Alù, and P. A. Huidobro, *Physical Review Letters* **125**, 127403 (2020).
- [32] A. Dikopoltsev, Y. Sharabi, M. Lyubarov, Y. Lumer, S. Tsesses, E. Lustig, I. Kaminer, and M. Segev, *Proceedings of the National Academy of Sciences* **119**, e2119705119 (2022).
- [33] J. R. Zurita-Sánchez, P. Halevi, and J. C. Cervantes-González, *Physical Review A* **79**, 053821 (2009).
- [34] See Supplementary Material at (the link) for more details on SI-1. Derivation of temporal Smith-Purcell radiation dispersion equation; SI-2. Simulation methods; SI-3. Energy band analysis for time grating; SI-4. Temporal Smith-Purcell radiation with high-energy electrons; SI-5. Comparison of temporal and spatial Smith-Purcell radiation; SI-6. Tuning radiation intensity through modulation amplitudes; SI-7. Temporal Smith-Purcell radiation with a temporal slab of finite thickness.
- [35] V. Pacheco-Peña and N. Engheta, *Nanophotonics* **9**, 379 (2020).
- [36] F. G. De Abajo, *Reviews of Modern Physics* **82**, 209 (2010).
- [37] S. Lu, A. Nussupbekov, X. Xiong, W. J. Ding, C. E. Png, Z.-E. Ooi, J. H. Teng, L. J. Wong, Y. Chong, and L. Wu, *Laser & Photonics Reviews* , 2300002 (2023).
- [38] S. Xi, H. Chen, T. Jiang, L. Ran, J. Huangfu, B.-I. Wu, J. A. Kong, and M. Chen, *Physical Review Letters* **103**, 194801 (2009).
- [39] Z. Duan, X. Tang, Z. Wang, Y. Zhang, X. Chen, M. Chen, and Y. Gong, *Nature Communications* **8**, 14901 (2017).
- [40] H. Chen and M. Chen, *Materials Today* **14**, 34 (2011).
- [41] F. Liu, L. Xiao, Y. Ye, M. Wang, K. Cui, X. Feng, W. Zhang, and Y. Huang, *Nature Photonics* **11**, 289 (2017).
- [42] J. G. Gaxiola-Luna and P. Halevi, *Physical Review B* **103**, 144306 (2021).
- [43] J. Gaxiola-Luna and P. Halevi, *Applied Physics Letters* **122** (2023).
- [44] Y. Ye, F. Liu, M. Wang, L. Tai, K. Cui, X. Feng, W. Zhang, and Y. Huang, *Optica* **6**, 592 (2019).
- [45] J. A. Kong, *New York* (1975).
- [46] J.-F. Zhu, C.-H. Du, F.-H. Li, L.-Y. Bao, and P.-K. Liu, *IEEE Access* **7**, 181184 (2019).
- [47] D. Zhang, Y. Zeng, Y. Tian, and R. Li, *Photonics Insights* **2**, R07 (2023).
- [48] T. Chlouba, R. Shiloh, S. Kraus, L. Brückner, J. Litzel, and P. Hommelhoff, *Nature* **622**, 476 (2023).
- [49] D. Zhang, Y. Zeng, Y. Bai, Z. Li, Y. Tian, and R. Li, *Nature* **611**, 55 (2022).
- [50] Y. Sharabi, E. Lustig, and M. Segev, *Physical Review Letters* **126**, 163902 (2021).
- [51] C. T. Phare, Y.-H. Daniel Lee, J. Cardenas, and M. Lipson, *Nature Photonics* **9**, 511 (2015).